

RESONANT WHIRLING OF TWO-PIECE PROPSHAFTS IN REAR-WHEEL-DRIVE CARS

1. Introduction

Many modern cars with rear-wheel drives have a two-piece, rather than the traditional one-piece, propshaft (or tail-shaft). The cars include Holden Commodores, Nissans and many European makes. The two-piece shaft requires less floor clearance, and hence a smaller floor tunnel, and does not suffer from the high-speed twisting resonances to which the one-piece shaft is susceptible.

The two-piece shaft is, however, susceptible to a lower speed, high load (high torque) phenomenon in which the propshaft whirls with increasing amplitude until its restraining rubber bush is fully compressed in its mounting bracket (see Figure 1), causing a **thump** sound. The whirling amplitude builds up periodically, so that a regular series of thumps is heard at a frequency of about 5 per second.

The effect is very sensitive to the properties of the rubber bush and to its temperature. Different designs of bush are used by different makers, each with the purpose of minimizing both the whirling problem and the transmission of other vibrations to the car body. GMH has a particular design which it would prefer not to vary, because of retooling costs. It can however vary the properties of the rubber material itself. By trial and error it has achieved rubber properties which control the whirling problem to an acceptable level under normal conditions. GMH posed the question, to the MISG, of **whether one can give theoretical guidelines for optimal rubber properties**. This might lead to improved control of the whirling problem. It would also be useful for new and modified propshafts, if it could replace the tedious trial and error process previously employed.

GMH were also anxious to gain a better understanding of the whirling phenomenon, and felt, with us, that a mathematical description of the phenomenon was a prerequisite for the study of the rubber properties.

The thumping phenomenon is observed at both 40 and 80 *kph* approximately, although the phenomenon had a different quality at these two speeds. The 2:1 ratio between these speeds suggests that a fundamental resonance and a harmonic resonance are responsible. Such multiple resonances are typical of non-linear oscillating systems, so we looked for non-linear driving forces.

The tail-shaft has a natural frequency of oscillation, in its rubber bush, of about 40*cps*. A prime candidate for exciting this oscillation was the Hooke joints

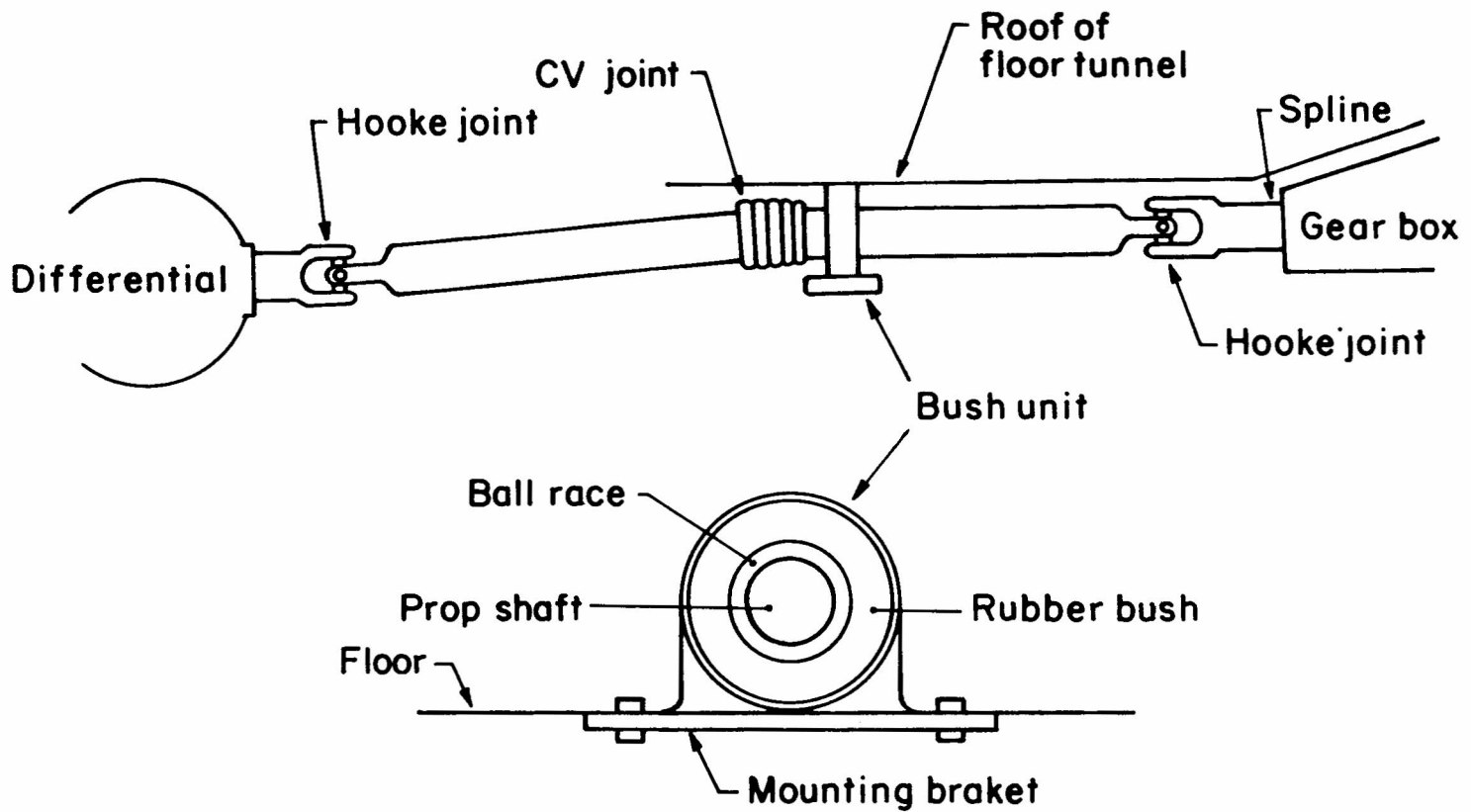


Figure 1: Sketch (not to scale) of a 2-piece drive shaft assembly, including detail of the rubber-bush-ballrace assembly.

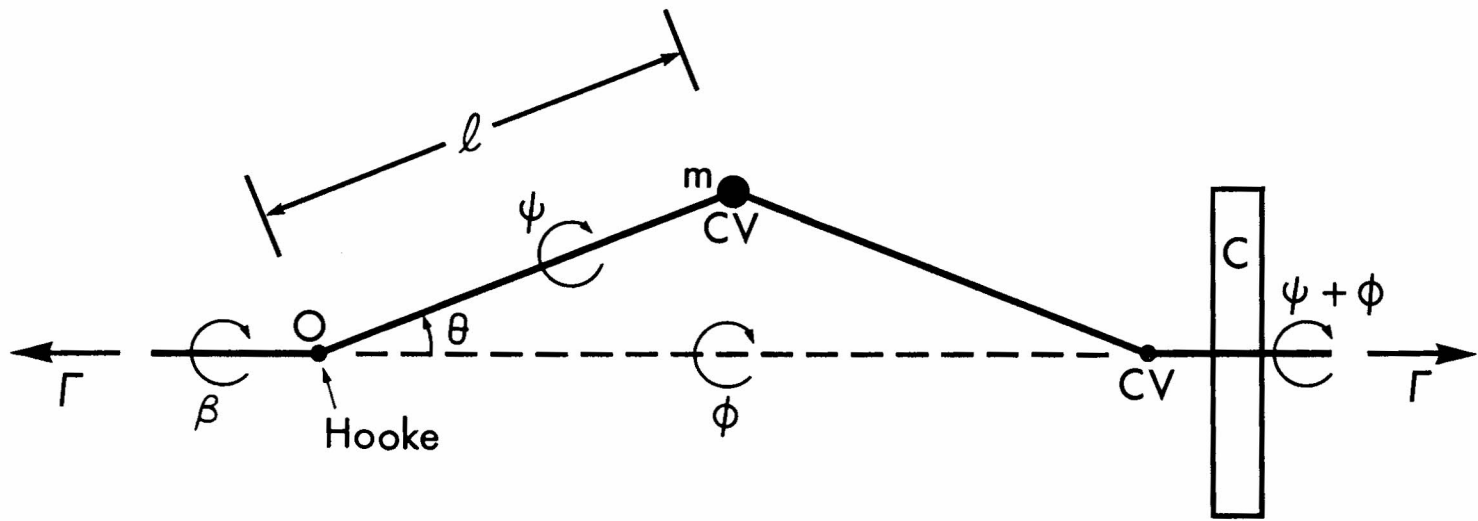


Figure 2: Schematic illustration of the simplified model showing various constants and variables.

(see Figure 1). These are known to impose oscillatory torques on the shafts they connect. The torques are known to excite torsional elastic oscillations in one-piece tail-shafts at higher speeds and frequencies (Zahradka 1973).

A miniature model of the tail-shaft assembly was built using Technic Lego, in a configuration resembling Figure 1. Hooke universal joints were used for all joints, rubber bands were used to approximate the rubber bush and the shaft was driven by an electric motor. The shaft-cum-rubber-band system had a natural frequency of about $20cps$. It was found possible to excite resonance at this frequency by tuning the speed of the motor precisely. When the shafts were all in a straight line, no such resonance was found. This rather primitive experiment showed that Hooke joints between angled shafts could be the driving force in the real system, and so the dynamics of this effect was studied. Other possible driving forces were discussed and eliminated to the group's satisfaction.

2. The dynamics of a simplified model

Figure 2 illustrates the simplified model that was analysed. The mass of the tail-shaft was replaced by a single point mass m coincident with the constant velocity (CV) joint. Real tail-shafts have moments of inertia and exhibit gyroscopic effects. There is no great difficulty in including such effects, but our primary aim was to focus on the crux of the resonance phenomena. Inclusion of all sorts of additional but inessential effects seemed likely to cloud the issue.

The rubber bush was taken as coincident with m . The front half of the shaft is nearly parallel to the gearbox shaft so that the front Hooke joint behaves like a CV joint. The real angle at this joint was given as no more than 1° , while the other joints were at varying angles of around 4° , so this approximation seemed satisfactory. However, for simplicity, we adopted the geometry shown in Figure 2, while retaining the front CV joint.

The angles θ, ϕ, ψ in Figure 2 are the Euler angles of rod Om relative to a fixed frame through O . The angle θ was taken as fixed because it was known that the spline joint tended to freeze up under load, preventing significant change in θ . A flywheel of moment of inertia C was located as shown. This was intended to represent the inertia of all the rotating car components connected to the tail-shaft itself. So C would include the rotating parts of the engine, gear box, differential, axles and the wheels (and, indirectly, the linear inertia of the car plus load, though decoupled somewhat by the rubber tyres).

Equal and opposite torques Γ are applied at the two ends of the system. No damping forces are included, because these seemed inessential to an understanding of the phenomenon.

The system has only 2 degrees of freedom, described by the 2 generalized coordinates ϕ and ψ . Evidently the system (with Γ 's included) is a self-contained conservative system. Energy can be exchanged between the mass m , the flywheel, the torques and the rubber bush. The whirling phenomenon would correspond to oscillations in ϕ .

A Lagrangian formulation of the dynamics is convenient because it deals easily with generalized coordinates and because it does not involve the rather complex forces and torques at the Hooke joints. Only the forces that do work (the Γ 's and the rubber bush forces) need be considered. The Lagrangian equations take the form (dots denote time derivatives).

$$\begin{aligned}\frac{d}{dt} \left(\frac{\partial T}{\partial \dot{\phi}} \right) - \frac{\partial T}{\partial \phi} &= -\frac{\partial V}{\partial \phi} \\ \frac{d}{dt} \left(\frac{\partial T}{\partial \dot{\psi}} \right) - \frac{\partial T}{\partial \psi} &= -\frac{\partial V}{\partial \psi}\end{aligned}\quad (1)$$

where T is the kinetic energy and V is the potential energy of the system. The flywheel has angular velocity $\dot{\psi} + \dot{\phi}$ shown in Figure 2. The mass m has linear velocity $\dot{\phi} l \sin \theta$ with l being the distance from O to m as shown in Figure 2. Thus

$$T = \frac{1}{2} m (\dot{\phi} l \sin \theta)^2 + \frac{1}{2} C (\dot{\psi} + \dot{\phi})^2 \quad (2)$$

We suppose, for simplicity, that the rubber bush is ideally elastic and exerts a force ks where k is a stiffness constant and $s = \phi l \sin \theta$ is the displacement of m along its circular path. The potential energy due to the torques Γ is the negative of the work done by the torques. Noting the angles in Figure 2 we thus have

$$V = \frac{1}{2} k (\phi l \sin \theta) + \Gamma (\psi + \phi - \beta) \quad (3)$$

A standard relation for Hooke joints is (Wagner and Cooney 1979).

$$\beta = \phi + \arcsin \left[\frac{\sin \psi}{(1 - \sin^2 \theta \cos^2 \psi)^{\frac{1}{2}}} \right] \quad (4)$$

For equations (1) we need

$$\frac{\partial \beta}{\partial \psi} = \frac{\cos \theta}{1 - \sin^2 \theta \cos^2 \psi} \quad (5)$$

Substituting (2), (3) and (5) in (1) gives

$$\begin{aligned}(m \ell^2 \sin^2 \theta) \ddot{\phi} + C(\ddot{\psi} + \ddot{\phi}) &= -(k \ell^2 \sin^2 \theta) \phi \\ C(\ddot{\psi} + \ddot{\phi}) &= [\cos \theta / (1 - \sin^2 \theta \cos^2 \psi) - 1] \Gamma\end{aligned}\quad (6)$$

We take initial conditions

$$\psi(0) = 0, \quad \dot{\phi}(0) = 0$$

with various $\phi(0)$ and $\dot{\psi}(0)$. Since θ is of order 4^0 , we can expand the sines and cosines and keep only terms up to θ^2 . Then equations (6) combine to give

$$\begin{aligned} \omega^{-2}\ddot{\phi} &= -\phi + A \cos(2\psi) \\ \omega^{-2}\ddot{\psi} &= \phi - B \cos(2\psi) \end{aligned} \tag{7}$$

where $\omega = (k/m)^{\frac{1}{2}}$ is the **natural frequency** of the system,

$$\begin{aligned} A &= \Gamma/(2k\ell^2), \\ B &= A(1 + m\ell^2\theta^2/C) \end{aligned} \tag{8}$$

A convenient simplification is to put $T = \omega t$. Then

$$\begin{aligned} \phi'' &= -\phi - A \cos(2\psi) \\ \psi'' &= \phi + B \cos(2\psi) \end{aligned} \tag{9}$$

where $(') = (d/dT)$.

The dimensionless constants A and B summarize the physical regime in which we are interested. For VN Commodores

$$\begin{aligned} k &\approx 10^6 N/m \\ \Gamma &\approx 290 Nm \\ \ell &\approx 1m \end{aligned}$$

whence

$$A \approx 1.5 \times 10^{-4}$$

We note that B/A measures the ratio of the moment of inertia of flywheel plus m to flywheel alone. Since C represents many inertial parts, we expect $C \gg m\ell^2\theta^2$, whence

$$A \approx B$$

Then (9) gives

$$\phi'' + \psi'' = 0$$

so that

$$\phi + \psi = N\tau$$

where $N = \dot{\psi}(0)/\omega$ and $\tau = T + \phi(0)/N$. Using Φ for ϕ we now have

$$\Phi'' = -\Phi + A \cos(2N\tau - 2\Phi). \tag{10}$$

This is the equation upon which our subsequent discussion is based. We see that it resembles a simple harmonic oscillation (SHO) with a forcing term of small amplitude A . Prior to resonance we would expect Φ to be small, so that

$$\Phi'' \approx -\Phi + A \cos(2N\tau). \quad (11)$$

This linear equation exhibits resonance at $N = \frac{1}{2}$, so we would expect resonance in (10) at this N . The non-linear Φ dependence in (10), however, gives a resonance which grows and develops in a fashion radically different from (11).

3. The resonant behaviour

Figure 3 gives a suite of solutions of (10) for a several values of N and $\Phi(0) = 0$ obtained by numerical computation using IMSL routine IVPRK. We took $A = 0.05$, larger than its true value, so that individual oscillations are clearer. We noted the expected resonance at $N = \frac{1}{2}$ (figure 3a) plus others at $N = \frac{1}{4}$ and $N = 1$ (Figure 3b). The resonances do not persist, but rather they grow and die away in periodic fashion. As N moves away from a resonant value, the period of this **envelope** decreases quite rapidly as does the amplitude (Figure 3c).

This periodic surging in the resonant behaviour seems quite close to GMH's description of the thumping phenomenon. The peak amplitudes are potential thumps, since the peaks occur at a frequency much less than N . We cannot make a more quantitative comparison at this stage because of the simplifications in our model.

The resonances can be derived theoretically as follows. In (10) we put $y = 2\Phi$, $\eta = 2N$ and $\alpha = 2A$, which gives

$$y'' + y = \alpha \cos(y - \eta\tau). \quad (12)$$

For $\alpha \ll 1$ and $\tau \ll 1/\alpha$ we can obtain a solution $y(\tau)$ in powers of α via the recursion

$$\begin{aligned} y_0 &= 0 \\ y''_{j+1} + y_{j+1} &= \alpha \cos(y_j - \eta\tau) \end{aligned} \quad (13)$$

for $j = 0, 1, 2, \dots$, with $y_j(0) = \dot{y}_j(0) = 0$. Thus

$$y''_1 + y_1 = \alpha \cos(\eta\tau)$$

with solution

$$y_1 = \frac{\alpha}{1 - \eta^2} [\cos(\eta\tau) - \cos \tau] \quad (14)$$

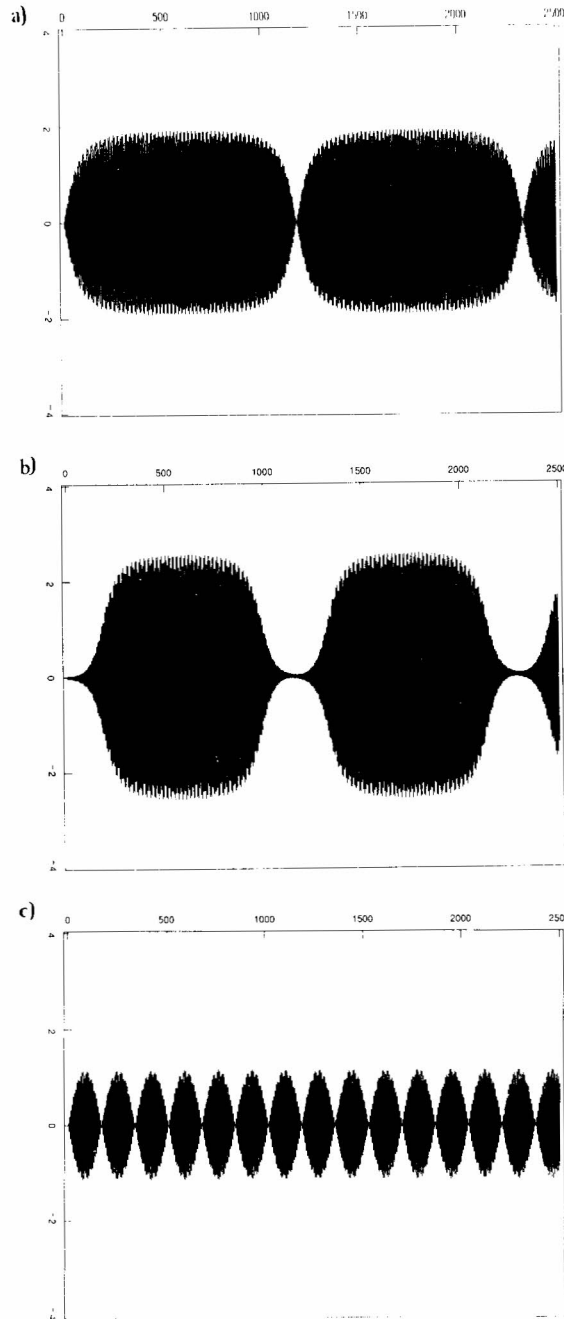


Figure 3: Resonant and near resonant oscillations Φ vs τ with $\Phi(0) = 0$, $\dot{\Phi}(0) = 0$. Case (a) is the fundamental resonance with $N = 0.5$ (engine angular velocity). Case (b) is the first overtone with $N = 1$. Case (c) has $N = 0.49$, just below resonant speed. The uneven peaks in Figures 3 and 4 are a result solely of the coarse time steps at which Φ is plotted.

This shows the expected **fundamental** resonance at $\eta = 1 (N = \frac{1}{2})$. The next iterate satisfies

$$y_2'' + y_2 = \alpha \cos(\eta\tau) - \alpha y_1 \sin(\eta\tau) + O(y_1^2) \quad (15)$$

$$= \alpha \cos(\eta\tau) + \frac{\frac{1}{2}\alpha^2}{1 - \eta^2} [\sin(2\eta\tau) - \sin(\eta + 1)\tau - \sin(\eta - 1)\tau] + O(\alpha^3). \quad (16)$$

The $O(\alpha^2)$ driving terms imply that y_2 has resonances at

$$\eta + 1 = 1, \quad 2\eta = 1 \quad \text{and} \quad \eta - 1 = 1$$

i.e. $\eta = 0, \frac{1}{2}$ and $2 (N = 0, \frac{1}{4}$ and $1)$. The values $N = \frac{1}{4}$ and 1 are the first undertone and first overtone of the fundamental resonance $N = \frac{1}{2}$. The coefficient α^2 indicates a more slowly growing resonance compared to the fundamental. This is consistent with Figure 3b. The $N = 0$ resonance is an artifact of the simplification leading to (10), which effectively gives the external system infinite inertia ($C = \infty$). Thus the system can have a spurious energy even when $N = 0$.

Since these solutions are valid only for small τ , they predict only the onset of resonance, not its later development.

It seems likely that the fundamental ($N = \frac{1}{2}$) and first overtone ($N = 1$) resonances correspond to the observed thumping phenomena at $40kph$ and $80kph$.

For $\Phi(0) \neq 0$ one finds other **modes** of oscillation. We illustrate in Figure 4 how the fundamental resonance, $N = \frac{1}{2}$, varies as $\Phi(0)$ increases. We shall classify these modes further in Section 4.

4. Asymptotic analysis

The technique developed by Krylov and Bogoliubov (see Bogoliubov and Metropolski 1961 (BM)) enables one to find the amplitude (and phase) of the envelopes of the solution curves, like those shown in Figures 3 and 4. First we write our equation in the notation of BM:

$$\ddot{x} + \omega^2 x = \varepsilon f(\nu t, x, \dot{x}) \quad (17)$$

with

$$f(T, x, \dot{x}) = \cos(T - x), \quad (18)$$

where $\varepsilon = 2\omega^2 A$, $x = 2\Phi$ and $\nu = 2\dot{\psi}(0)$. BM represent solutions of (17) in the form

$$x(t) = a(t) \cos[\nu t + \Theta(t)] + O(\varepsilon) \quad (19)$$

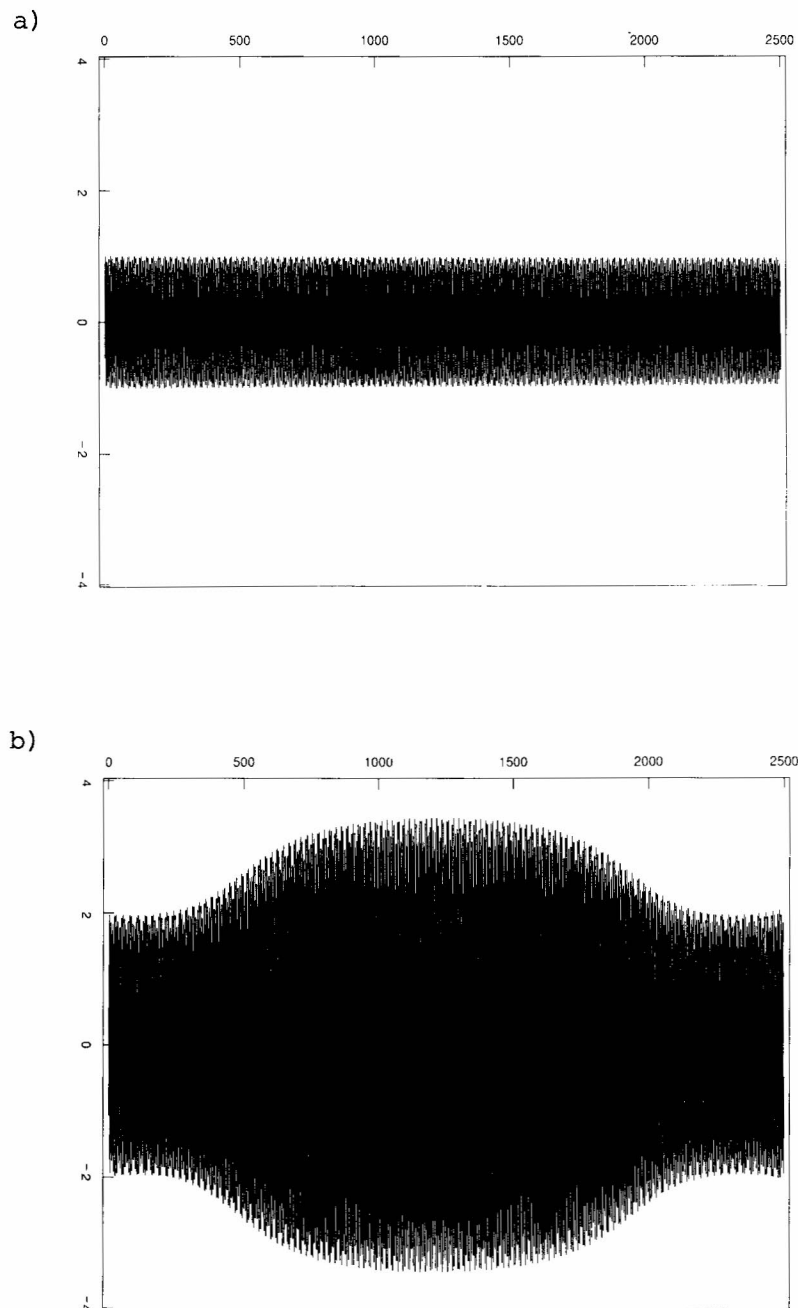


Figure 4: Fundamental resonant oscillations $N = 0.5$, $\dot{\Phi}(0) = 0$. Case (a) illustrates mode 1 with $\Phi(0) = 1.0$. Case (b) illustrates mode 2 with $\Phi(0) = 2.0$ (cf Figures 5 and 6). Case (a) is close to the constant amplitude case of mode 1.

Typically one finds that $a(t)$ and $\Theta(t)$ vary slowly compared to $\cos(\nu t)$, so they describe the envelope of the fast oscillations. BM, (14.4), obtain an asymptotic expansion for a and Θ in powers of ε . To first order these are given by (BM (14.25) with $p = q = 1$)

$$\frac{da}{dt} = -\frac{\varepsilon}{\nu} \sum_{\sigma=-\infty}^{\infty} e^{i\sigma\Theta} F_{\sigma}(a) \quad (20)$$

$$\frac{d\Theta}{dt} = \omega - \nu - \frac{\varepsilon}{a\nu} \sum_{\sigma=-\infty}^{\infty} e^{i\sigma\Theta} G_{\sigma}(a) \quad (21)$$

where

$$F_{\sigma}(a) = \frac{1}{4\pi^2} \int_0^{2\pi} d\theta \int_0^{2\pi} d\psi \sin \psi e^{-i\sigma(\psi-\theta)} f_0(a, \theta, \psi) \quad (22)$$

$$G_{\sigma}(a) = \frac{1}{4\pi^2} \int_0^{2\pi} d\theta \int_0^{2\pi} d\psi \cos \psi e^{-i\sigma(\psi-\theta)} f_0(a, \theta, \psi) \quad (23)$$

and (BM (14.4))

$$\begin{aligned} f_0(a, \theta, \psi) &\equiv f(\theta, a \cos \psi, -\frac{1}{2}a\nu \sin \psi) \\ &= \cos(\theta - a \cos \psi) \end{aligned} \quad (24)$$

Note that the integration variables θ and ψ bear *no relation* to our original Euler angles.

We evaluate the integrals in stages. First, for F_{σ} , we need

$$\begin{aligned} \frac{1}{2\pi} \int_0^{2\pi} d\theta e^{-i\sigma(\psi-\theta)} \cos(\theta - a \cos \psi) &= e^{i\sigma(a \cos \psi - \psi)} \frac{1}{2\pi} \int_0^{2\pi} d\phi e^{i\sigma\phi} \cos \phi \\ &= \frac{1}{2}(\delta_{\sigma,1} + \delta_{\sigma,-1}) e^{i\sigma(a \cos \psi - \psi)} \end{aligned} \quad (25)$$

where $\delta_{i,j}$ is the Kronecker delta. Then we need

$$\begin{aligned} \bar{F} &= \frac{1}{2\pi} \int_0^{2\pi} d\psi \sin \psi e^{i\sigma(\cos \psi - \psi)} \\ &= \frac{1}{2\pi} \int_0^{2\pi} d\psi \sin \psi [\cos(\sigma\psi) - i \sin(\sigma\psi)] [\cos(\sigma a \cos \psi) + i \sin(\sigma a \cos \psi)] \\ &= \frac{1}{4\pi} \int_0^{2\pi} d\psi [\sin(\sigma a \cos \psi) \cos\{(\sigma - 1)\psi\} - \sin(\sigma a \cos \psi) \cos\{(\sigma + 1)\psi\} \\ &\quad - i \cos(\sigma a \cos \psi) \cos\{(\sigma - 1)\psi\} + i \cos(\sigma a \cos \psi) \cos\{(\sigma + 1)\psi\}] \end{aligned} \quad (26)$$

We have the standard integrals (Prudnikov *et al* 1986, para. 2.5.27, p440)

$$\left. \int_0^{2\pi} dx \begin{array}{l} \sin(z \cos x) \\ \cos(z \cos x) \end{array} \right\} \sin(nx) = 0$$

and

$$\int_0^{2\pi} dx \left. \begin{array}{l} \sin(z \cos x) \\ \cos(z \cos x) \end{array} \right\} \cos(nx) = \left. \begin{array}{l} \sin(n\pi/2) \\ \cos(n\pi/2) \end{array} \right\} J_n(z)$$

for all integers n , where the J_n are Bessel functions. Now

$$\bar{F} = \frac{1}{2}i \left[e^{i(\sigma+1)\pi/2} J_{\sigma+1}(\sigma a) - e^{i(\sigma-1)\pi/2} J_{\sigma-1}(\sigma a) \right] \quad (27)$$

and (22), (25) and (27) give

$$F_\sigma(a) = \frac{1}{4}i(\delta_{\sigma,1} - \delta_{\sigma,-1}) \left[e^{i(\sigma+1)\pi/2} J_{\sigma+1}(\sigma a) - e^{-i(\sigma-1)\pi/2} J_{\sigma-1}(\sigma a) \right] \quad (28)$$

Thus (20) has contributions only from $\sigma = +1$ and -1 . Noting that $J_{-n}(-z) = J_n(z)$ we eventually have

$$\frac{da}{dt} = -\frac{\varepsilon}{2\nu} [J_0(a) + J_2(a)] \sin \Theta. \quad (29)$$

By a similar procedure, (21) reduces to

$$\frac{d\Theta}{dt} = \omega - \nu - \frac{\varepsilon}{2\nu a} [J_0(a) - J_2(a)] \cos \Theta \quad (30)$$

Noting that (Abramowitz and Stegun 1965)

$$J_0(a) - J_2(a) = 2J_1'(a)$$

$$J_0(a) + J_2(a) = 2J_1(a)/a$$

we can write (29) and (30) in the form

$$\begin{aligned} \frac{da}{dt} &= \frac{1}{a} \frac{\partial H}{\partial \Theta} \\ \frac{d\Theta}{dt} &= -\frac{1}{a} \frac{\partial H}{\partial a} \end{aligned} \quad (31)$$

where

$$H(a, \theta) = \frac{\varepsilon}{\nu} J_1(a) \cos \Theta + \frac{1}{2}(\nu - \omega)a^2 \quad (32)$$

Thus (31) is a Hamiltonian system with generalized position and momentum variables $\frac{1}{2}a^2$ and Θ (or $-\Theta$ and $\frac{1}{2}a^2$) respectively. The practical consequence is that H is a constant of the *motion* (or first integral) and (31) can be solved analytically.

The *motion* can be described qualitatively as follows. Put

$$H(a, \Theta) = \text{constant.}$$

Then for the fundamental resonance $\nu = \omega$ ($N = \frac{1}{2}$) we have

$$J_1(a) \cos \Theta = K$$

for constant K . The resulting family of curves in the (a, Θ) plane are shown in Figure 5 for various K . The particular cyclic path followed by the system depends on the choice of $\Phi(0)$. This shows how one can obtain oscillations of the type illustrated in Figure 4.

Figure 6 shows a numerical solution of the envelope equations (31) with $a(0) = 0.01$ and $\Theta = 0$. The resulting envelope is evidently very close to the simulation Figure 3a. The envelope equations do not admit a solution with $a(0) = 0$, but $a(0)$ can be very small, so one can get arbitrarily close to the $\Phi(0) = 0$ simulation.

The asymptotic analysis thus explains why the resonance like Figure 3a has an oscillating envelope. For more detail, note that (31) implies, for $\nu = \omega$,

$$\frac{d^2 a}{dt^2} = \frac{\varepsilon^2}{\nu^2} \left[\frac{J_1(a)J_1'(a)}{a^2} - \frac{J_1(a)^2}{a^3} \sin \Theta \right]$$

At maximum and minimum a , (31) implies $\Theta = 0$. Thus

$$\frac{d^2 a}{dt^2} = \frac{\varepsilon^2}{\nu^2} \cdot \frac{J_1(a)J_1'(a)}{a^2} \sim \begin{cases} \frac{\varepsilon}{\nu^2} \cdot \frac{2}{a} & \text{as } a \rightarrow 0 \\ 0- & \text{as } a \rightarrow a_1 \end{cases}$$

where a_1 is the first zero of J_1 . Thus $a(t)$ has a large positive curvature at its minimum and a small negative curvature at its maximum. In the case $\Phi(0) = 0$, large becomes $+\infty$ and small becomes 0; hence Figure 3a.

The peak amplitude \bar{a} of the oscillations at frequency ν and $\Phi(0) = 0$ is obtained by setting

$$H(\bar{a}, 0) = 0$$

This quadratic equation in ν has solution

$$\nu = \frac{1}{2}\omega + \frac{1}{2}\{\omega^2 - 8\varepsilon J_1(\bar{a})/\bar{a}^2\}^{\frac{1}{2}}$$

Including $\bar{a} < 0$ solutions and plotting $|\bar{a}|$ against ν gives Figure 7. This shows the modes obtained in Figures 4 and 5 and how they are modified when ν differs from ω . We see that the higher amplitude modes can exist only within sharply

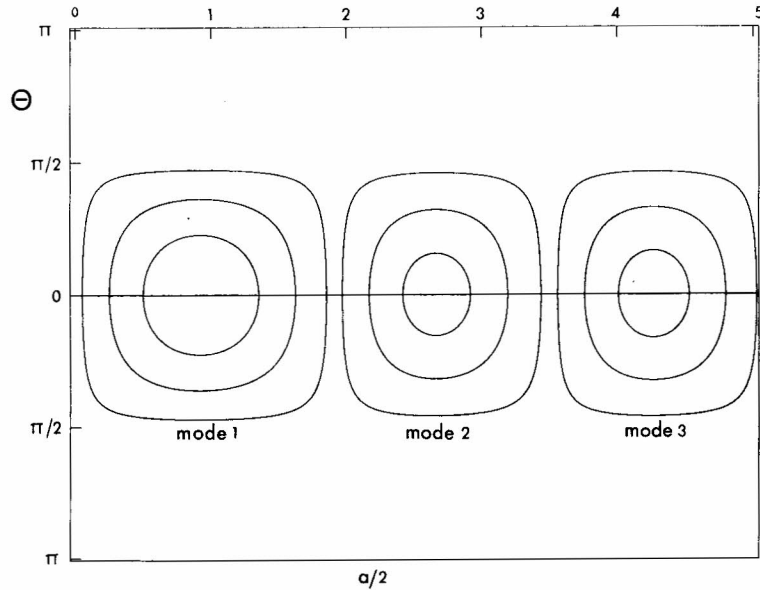


Figure 5: Variation of amplitude $\frac{1}{2}a$ of the envelope versus its phase Θ at the fundamental frequency $N = 0.5$. These curves, obtained from the method of averaging (Krylov-Bogoliubov), are very close to simulation results.

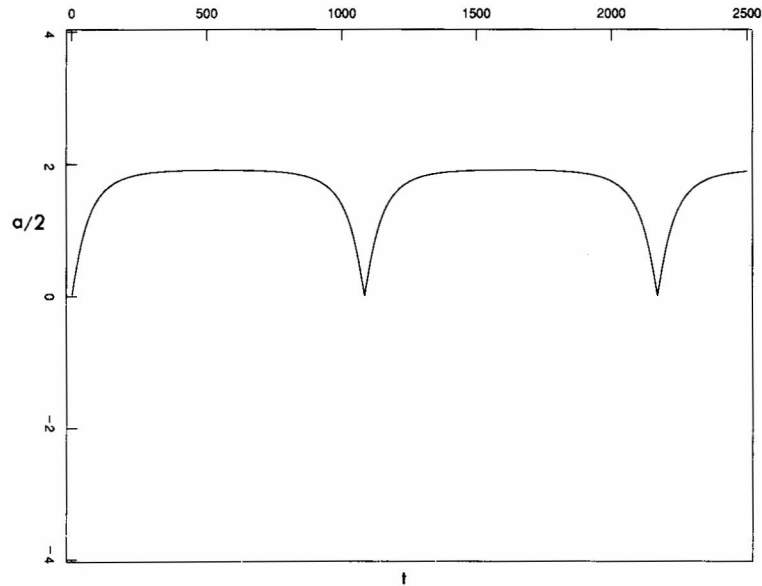


Figure 6: The envelope $\frac{1}{2}a$ vs t as predicted by the KB theory with $a(0) = 0.01$ and $\Theta(0) = 0$. The result is close to the envelope of Figure 3(a).

defined intervals of ν values centred on ω . The width of these intervals decreases for large \bar{a} , like

$$J_1(\bar{a})/\bar{a}^2 \sim 1/\bar{a}^{\frac{5}{2}}$$

We have not examined whether or how these modes, other than the lowest amplitude mode, might be excited in a practical situation. They would seem to require a large, abrupt input of energy directly to the Φ motion, when the frequency is close to ω . We know of no mechanism which might achieve this.

5. Conclusions

We have devised and analysed a simplified mathematical model of the whirling and thumping phenomenon. The model shows that Hooke universal joints can cause whirling (ϕ oscillations) in the propshaft at its natural frequency and at overtone and undertone frequencies. The observed thumping at $40kph$ and $80kph$ seem likely to correspond to the 2 largest resonances: the fundamental (natural) frequency and its first overtone.

The rubber property in our model is the linear elastic stiffness constant k of the bush. There is the obvious dependence of the resonant engine speeds $\frac{1}{4}\omega$, $\frac{1}{2}\omega$ and ω (radians per second) on k through $\omega = (k/m)^{\frac{1}{2}}$. Increasing stiffness pushes up these speeds. Further, equations (31) show that the thumping frequency (i.e. the envelope frequency) is proportional to ε and hence to Γ/k . So increasing stiffness causes the frequency of thumping to decrease. We note however that thumping (envelope) frequency is very sensitive to departures from resonant frequencies (Figure 3c) and to initial conditions $\Phi(0)$ and $\Phi'(0)$.

The time and data available at the MISG did not permit us to study this central practical problem in more detail; so it remains to find rubber properties in the central bush that minimize the severity of the phenomena. However the study reported here shows that this problem can be analysed using the following techniques.

1. A Lagrangian formulation of the basic dynamics, incorporating more realistic inertial and gyroscopic terms and rubber parameters.
2. A numerical solution of the resulting differential equations using an IMSL program.
3. The iteration scheme of Section 3 to locate resonances of first, second, etc order.

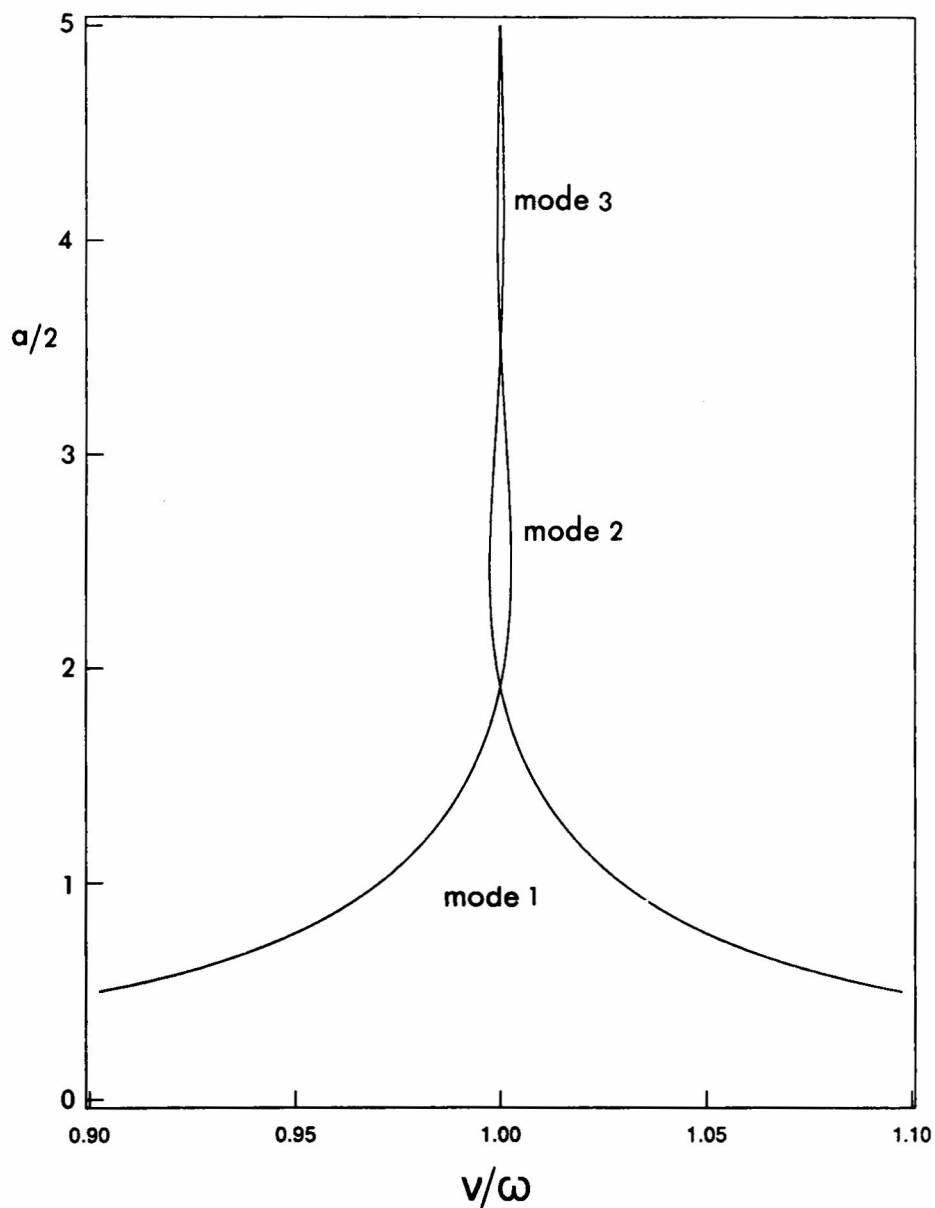


Figure 7: Variation of envelope amplitude $\frac{1}{2}a$ with engine speed $\dot{\psi}(0)(= \frac{1}{2}\nu)$. Note that models, other than mode 1, are confined to a very narrow range of engine speeds around the fundamental resonant speed $\frac{1}{2}\omega$.

4. The Krylov-Bogoliubov technique (Section 4) to directly obtain the dependence of resonant amplitudes and thumping (envelope) frequencies on rubber properties.

These techniques have wide application to problems involving oscillations of non-linear systems (Bogoliubov & Metropolski, 1961 and Hagedorn, 1981).

References

- Abramowitz, M. and Stegun, I.A. (1965) Handbook of Mathematical Functions. 5th edition. New York: Dover.
- Bogoliubov, N.N and Metropolski, Y.A. (1961) Asymptotic Methods in the Theory of Non-linear Oscillations. New York: Gordon and Breach.
- Hagedorn, P. (1981) Non-linear Oscillations. Oxford: Clarendon.
- Prudnikov, A.P., Brychkov, Yu, A. and Marichev, O.I. (1986) Integrals and Series Vol I, New York: Gordon and Breach.
- Wagner, E.R. and Cooney, C.E. (1979) Cardan and Hooke universal joint. Section 3.1.1, p39 in Universal Joint and Driveshaft Design Manual. Advances in Engineering, Series 7. Published by the Society of Automotive Engineers, New York.
- Zahradka, J. (1973) Torsional vibrations of a non-linear driving system with Cardan shafts. *J. Sound and Vibration*, **26**(4), 533-550.